Available on the CERN CDS information server **CMS PAS SUS-16-050**

CMS Physics Analysis Summary

Contact: cms-pag-conveners-susy@cern.ch 2017/05/08

Search for supersymmetry using hadronic top quark tagging in 13 TeV pp collisions

The CMS Collaboration

Abstract

A search is presented for supersymmetry in all-hadronic events with missing transverse momentum and tagged top quarks. The data sample was collected with the CMS detector at the LHC and corresponds to an integrated luminosity of 35.9 fb^{-1} of proton-proton collisions at a center-of-mass energy of 13 TeV. Search regions are defined using the multiplicity of bottom and top quark candidates, the presence of an imbalance in transverse momentum, and the hadronic energy in the event. With no statistically significant excess of events observed beyond the expected contributions from the standard model, we set exclusion limits at the 95% confidence level on the masses of new particles in the context of simplified models of direct and gluino-mediated top squark production. For direct top squark production with decays to a top quark and a neutralino, top squark masses up to 1020 GeV and neutralino masses up to 430 GeV are excluded. Gluino masses up to 2040 GeV and neutralino masses up to 1150 GeV are excluded for models of gluino pair production where each gluino decays to a top-antitop quark pair and a neutralino.

1 Introduction

The discovery of the standard model (SM) Higgs boson [1–3] at the CERN LHC [4] has been the most groundbreaking work of the LHC to date. However, its mass of 125 GeV [5] can only be explained with the SM with large fine tuning in the quantum loop corrections of the Higgs boson mass. The most popular model which contains an explanation for the Higgs boson mass to be finite and stable, without fine tuning, is the proposed expansion of the Poincaré symmetries of the SM to include additional "fermionic" symmetries, called supersymmetry (SUSY) [6–14]. The consequences of these new symmetries is a superpartner ("sparticle") for each SM particle with the same quantum numbers except for spin, which differs by a half-integer. SUSY explains why the Higgs boson mass is at the electroweak scale because the contributions from each SM particle to the Higgs-mass loop corrections is canceled by their superpartner. As no superpartners have been observed with masses equal to their SM partners, supersymmetry must be a broken symmetry at some level. In this scenario, the finite Higgs boson mass is maintained, but the precept of naturalness would suggest that the scale of new physics which cancels the quadratically divergent Higgs boson mass terms must be of the order of the mass itself. In particular, the masses of the top squark and gluino (the superpartner of the gluon) must not be significantly heavier than the Higgs boson mass to maintain the naturalness of SUSY. This motivates searches for the top squarks and gluinos with masses around the TeV scale as an important indicator of "natural" SUSY models which explain the Higgs boson mass and characteristic scale of SUSY with minimal fine tuning [15].

Motivated by the above argument, we perform a search for top squarks, produced either directly or through gluino decays. The top squarks then decay to a stable neutralino $\widetilde{\chi}_1^0$, which is assumed to be the LSP, and a SM quark, the latter of which can further decay. Depending on the mass of the top squark and the mixing angles in the decays, most or all of the top squarks will decay to top quarks. Additionally, depending on whether the top squarks are pair produced or produced through gluino decays, there can be between two and four top quarks in the final state. Based upon this, a novel algorithm to identify multiple hadronically-decaying top quarks over a wide range of p_{T} is employed to enhance the sensitivity to models with top quarks in the decay chain. This algorithm uses three separate top quark decay topologies (in order of increasing Lorentz boost): three distinct jets with no more than one b jet, two distinct jets representing the W boson and the b quark, or a fully merged case in which the otherwise distinct jets are identified by the jet clustering algorithm as a single jet. This allows it to maintain high efficiency over a wide range of top quark p_{T}.

This search is performed using a sample of multijet events with a large imbalance in transverse momentum (p_{T}) collected by the CMS experiment in 2016 and corresponding to an integrated luminosity of 35.9 fb^{-1} of proton-proton collisions at a center-of-mass energy of 13 TeV. Searches for top squarks and gluinos have already been performed at the LHC using a sample of proton-proton collisions at $\sqrt{s} = 13\,\mathrm{TeV}$ collected during 2015, corresponding to 2–3 fb^{-1}, and no evidence for beyond-the-SM physics has been found. Lower limits have been placed on the top squark, gluino and LSP masses within simplified models of SUSY (SMS) [16–20]. For models of direct top squark production, where each top squark decays to a top quark and a $\widetilde{\chi}_1^0$, top squark masses up to 830 GeV and $\widetilde{\chi}_1^0$ masses up to 300 GeV have been excluded [21–24]. For models of gluino pair production, where each gluino decays to $\mathrm{t\bar{t}}\widetilde{\chi}_1^0$ via an off-shell top squark, gluino masses up to 1760 GeV and $\widetilde{\chi}_1^0$ masses up to 950 GeV have been excluded [22, 23, 25–30].

Events are selected that contain large missing transverse momentum ($E_{\mathrm{T}}^{\mathrm{miss}}$), at least four jets, at least one jet identified as originating from the hadronization of a b quark ("b jet"), at least one identified top quark decay, and no identified leptons. Exclusive search regions are defined

using several event properties, including the number of identified b jets N_b, the number of top quark candidates N_t, the missing transverse momentum E_T^{miss}, the sum of hadronic jet p_T H_T, and the stranverse mass calculated using reconstructed top quarks M_{T2}. With this selection, the predominant source of SM background originates either from top-antitop quark pair ($t\bar{t}$) production or from W+jets production. Specifically events in which leptonic W boson decay yields both a high-momentum neutrino, which generates true missing transverse momentum, and a charged lepton that is not identified or reconstructed or out-of-acceptance. Events in which a Z boson, produced in association with jets, decays to neutrinos ($Z \to \nu\bar{\nu}$) also provide a significant contribution to the SM background. Quantum chromodynamics (QCD) multijet events can also contribute when mismeasurement of jet p_T creates large missing transverse momentum. Additional small background sources include single top quark production, vector boson production, and $t\bar{t}$ events with a Z boson.

2 The CMS detector

The CMS detector is built around a superconducting solenoid of 6 m internal diameter, providing a magnetic field of 3.8 T. Within the solenoid volume are a silicon pixel and strip tracker, a lead tungstate crystal electromagnetic calorimeter (ECAL), and a brass and scintillator hadron calorimeter (HCAL). The tracking detectors cover $|\eta| < 2.5$. The ECAL and HCAL, each composed of a barrel and two endcap sections, extend over a pseudorapidity range $|\eta| < 3.0$. Forward calorimeters on each side of the interaction point encompass $3.0 < |\eta| < 5.2$. Muons are identified and measured within $|\eta| < 2.4$ by gas-ionization detectors embedded in the steel flux-return yoke outside the solenoid. The first level of the CMS trigger system, composed of custom hardware processors, uses information from the calorimeters and muon detectors to select the most interesting events in a fixed time interval of less than 4 μs. The high-level trigger processor farm further decreases the event rate from around 100 kHz to less than 1 kHz before data storage. A more detailed description of the CMS detector, together with a definition of the coordinate system used and the relevant kinematic variables, can be found in Ref. [31].

3 Event reconstruction and simulation

Events are reconstructed using the particle-flow (PF) algorithm [32, 33], which reconstructs charged hadrons, neutral hadrons, photons, muons, and electrons using information from all subdetectors. The negative vector sum of the transverse momentum of all particles reconstructed in the event is denoted by $\vec{p}_T^{miss}$ and the missing transverse momentum E_T^{miss} is its magnitude. All photons and neutral hadrons in an event, together with charged particles that originate from the primary interaction, are clustered into jets using the anti-k_T clustering algorithm with size parameter 0.4 (AK4) [34]. Neutral particles from overlapping pp interactions ("pileup") and particles from the underlying event are subtracted on an event-by-event basis using the FASTJET technique [35, 36]. The energy and momentum of each jet is corrected using factors derived from simulation, and for jets in data, an additional residual energy-momentum correction is applied to account for differences in the jet energy-momentum scales [37] between simulation and data. Only jets with $p_T > 30$ GeV and $|\eta| < 2.4$ (tight) or $|\eta| < 5$ (loose) are used in this search. The scalar sum of the transverse momenta of the jets (within $|\eta| < 2.4$) is denoted by H_T.

For this analysis, a tight jet ($|\eta| < 2.4$) is considered a b quark jet (b-tagged) if it passes the medium operating point requirements of the "Combined Secondary Vertex" (CSVv2) method [38, 39]. The b quark identification efficiency ranges 60–70% for jet p_T 20–400 GeV. The probabil-

ity of a jet originating from a light quark or gluon to be misidentified as a b quark jet is 1.4%, averaged over p_T in $t\bar{t}$ events [39].

In addition to AK4 jets discussed above, jets clustered using the anti-k_T algorithm with size parameter 0.8 (AK8) are also used for top quark reconstruction and identification, as discussed below in Section 4.1. Inputs to the "fat" AK8 jet reconstruction are provided by the event reconstruction approach called "pileup per particle identification" (PUPPI) [40], which uses local shape information, event pileup properties, and tracking information to reduce the effect of pileup on reconstructed jets.

To obtain a sample of all-hadronic events, events with isolated electrons and muons are vetoed. Muons are reconstructed by matching tracks in the muon detectors to compatible track segments in the silicon tracker, and are required to have $p_T > 10\,\text{GeV}$ and be within $|\eta| < 2.4$. Electron candidates are reconstructed starting from a cluster of energy deposited in the ECAL that is then matched to a track in the silicon tracker. Electron candidates are required to have $p_T > 10\,\text{GeV}$ and satisfy $|\eta| < 1.44$ or $1.56 < |\eta| < 2.5$ to avoid the transition region between the ECAL barrel and endcap. Muon and electron candidates are required to originate within 2 mm of the beam axis in the transverse plane. The isolation of electron and muon candidates is defined as the $\sum p_T$ of PF candidates in a cone of radius $\Delta R = \sqrt{(\Delta\eta)^2 + (\Delta\phi)^2}$ around the candidate's trajectory. The cone size ranges from 0.05 to 0.2 depending on the lepton p_T. The isolation sum is corrected for contributions originating from pileup interactions using an estimate of the pileup energy in the cone. Electron and muon candidates are considered to be isolated if their relative isolation, i.e. the ratio of the isolation sum to the candidate p_T, is less than 0.1 and 0.2, respectively.

In order to further reduce the contribution from background events with low-p_T leptons originating from leptonic W boson decays, an additional veto on the presence of isolated tracks is applied. This veto reduces the overall background from leptonic W boson decays by about 40%. These tracks are required to have $p_T > 5\,\text{GeV}$, $|\eta| < 2.5$, and relative track isolation less than 0.2. This is the same as the relative isolation described above except that it is computed only with charged PF candidates within a fixed cone of $\Delta R = 0.3$ around the track. In order to preserve signal efficiency, events are vetoed only when the transverse mass (M_T) of the isolated track-E_T^{miss} system is less than 100 GeV to be consistent with W boson decay. The transverse mass is defined as

$$M_T(\text{track}, \vec{p}_T^{\,\text{miss}}) = \sqrt{2 \cdot p_T^{\text{track}} \cdot E_T^{\text{miss}} \cdot (1 - \cos\Delta\phi)}\ , \tag{1}$$

where p_T^{track} is the track p_T and $\Delta\phi$ is the azimuthal separation between the isolated track and $\vec{p}_T^{\,\text{miss}}$.

Following the veto on the presence of isolated electrons and muons, a significant fraction of the remaining SM background originates from events with hadronically-decaying τ leptons (τ_h). In order to reduce this background contribution, a veto is placed on the presence of isolated charged hadron PF candidates in the tracker volume with $p_T > 10\,\text{GeV}$ that are consistent with τ_h decays. The τ_h candidate-E_T^{miss} system is also required to have a transverse mass $M_T(\tau_h, \vec{p}_T^{\,\text{miss}}) < 100\,\text{GeV}$. Candidates satisfying the selection on $M_T(\tau_h, E_T^{\text{miss}})$ are categorized as being isolated if their relative track isolation is less than 0.1.

Monte Carlo (MC) simulated event samples are used to study the properties of the SM background processes as well as the signal models. The MADGRAPH5_AMC@NLO v2.2.2 generator [41] is used in leading-order (LO) mode to simulate events originating from various processes including $t\bar{t}$ production, W+jets with $W \to \ell\nu$ decays, Z+jets with $Z \to \nu\bar{\nu}$ decays,

Drell–Yan (DY)+jets, QCD multijet, gluino pair production, and top squark pair production. The generation of these processes is based on LO parton distribution functions (PDFs) using NNPDF3.0 [42]. Single top quark events produced in the tW channel are generated with the next-to-leading-order (NLO) POWHEG v1.0 [43–46] generator. Rare SM processes, such as $\mathrm{t\bar{t}Z}$ and $\mathrm{t\bar{t}W}$, are generated at NLO accuracy with the MADGRAPH5_AMC@NLO v2.2.2 program. Both single top quark production and rare SM processes are generated using NLO NNPDF3.0 PDFs. Parton showering and hadronization is simulated with PYTHIA v8.205 [47] using underlying-event tune CUETP8M1 [48].

The CMS detector response is simulated using a GEANT4-based model [49] for SM background processes and a dedicated fast simulation package [50] for signal processes, where a large number of signal model scenarios are needed. The fast simulation is tuned to provide results that are consistent with those obtained from the full GEANT4-based simulation. Event reconstruction is performed in the same manner as for collision data.

The signal production cross sections are calculated using NLO plus next-to-leading-logarithm (NLL) calculations [51]. The most precise available cross section calculations are used to normalize the SM simulated samples, corresponding to NLO or next-to-NLO accuracy in most cases [41, 52–58].

The simulation is corrected to account for discrepancies between data and simulation in the lepton selection efficiency and the b tagging efficiency. The uncertainties corresponding to these corrections are propagated to the predicted SM yields in the search regions. Differences in the efficiencies for selecting isolated electrons and muons are measured in $\mathrm{Z} \to \ell\ell$ events. Correction factors and their uncertainties for the b tagging efficiency are derived using multijet- and $\mathrm{t\bar{t}}$-enriched event samples and are parametrized by the jet kinematics [39].

4 Analysis description

This analysis is designed for maximum sensitivity to models with top quarks in the decay chains of SUSY particles. For direct top squark pair production, we consider one decay scenario within the SMS framework, denoted by "T2tt", in which each $\widetilde{\mathrm{t}}$ decays via a top quark: $\widetilde{\mathrm{t}} \to \mathrm{t}\widetilde{\chi}_1^0$, in which $\widetilde{\chi}_1^0$ is the LSP. We also consider a model of gluino-mediated top squark production, denoted by "T1tttt", where the gluino decays to top quarks via an off-shell top squark: $\widetilde{\mathrm{g}} \to \mathrm{t\bar{t}}\widetilde{\chi}_1^0$. This model is complementary to the direct top squark production because it provides sensitivity to scenarios containing a gluino which is kinematically accessible but the top squark is too heavy to be produced directly.

Another scenario, denoted by "T5ttcc", features on-shell top squarks in the decay chain with a mass difference between top squark and LSP assumed to be $\Delta m(\widetilde{\mathrm{t}}, \widetilde{\chi}_1^0) = 20\,\mathrm{GeV}$. For this model, the gluino decays to a top quark and a top squark, $\widetilde{\mathrm{g}} \to \mathrm{t\bar{t}}\widetilde{\mathrm{t}}$, and the top squark decays to a charm quark and an LSP, $\widetilde{\mathrm{t}} \to \mathrm{c}\widetilde{\chi}_1^0$. This model again serves as a complement to the direct search by providing sensitivity to very light top squarks, which would not decay to on-shell top quarks.

These scenarios, which are illustrated in Fig. 1, share similar final states, containing two neutralinos and up to four top quarks. Since the $\widetilde{\chi}_1^0$ is stable and only interacts weakly, it does not produce a signal in the detector. Therefore, $E_{\mathrm{T}}^{\mathrm{miss}}$ is one of the most important discriminators between signal and SM background, especially for models with large mass differences between the top squark or gluino and the $\widetilde{\chi}_1^0$. Since top quarks decay almost exclusively to a b quark and a W boson, each hadronically decaying top quark can result in up to three identified jets,

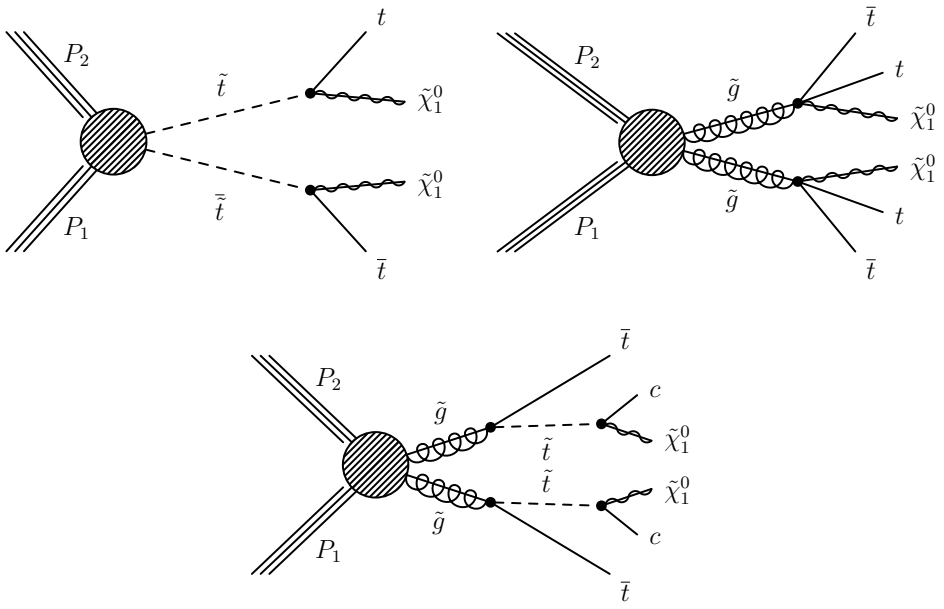

Figure 1: Diagrams representing the simplified models of direct and gluino-mediated top squark production considered in this study: the T2tt model (top left) with top squark decay via a top quark, and the T1tttt model (top right) where the gluino decays to top quarks and the LSP via an off-shell top squark, and the T5ttcc model (bottom) where the gluino decays to an on-shell top squark, which decays to a charm quark and the LSP.

depending on the top quark p_T and jet size.

4.1 Top quark reconstruction

As a central feature of the analysis, the top quark tagging algorithm is designed to give the best possible efficiency over the full range of top quark p_T seen in the signal models of interest. Traditional top quark tagging algorithms [59, 60] generally focus solely on identifying top quark decays which are boosted into a single large jet cone. A popular jet reconstruction algorithm uses jets clustered with the AK8 algorithm along with subjet information from the AK8 jet. These top quark tagging algorithms are very effective in the p_T range where the top quark boost is sufficiently high so that all three decay products are collimated into a single jet. However, at low top quark p_T ($< 400\,\text{GeV}$) a much larger cone must be used to capture the decay products of the top quark. Another approach to reconstruction of top quarks with low p_T is a "resolved" tagging algorithm that combines individual jets reconstructed with the AK4 algorithm. To get the best efficiency over a wide range of top quark p_T, this analysis uses a combination of both types of algorithms. In addition, we also consider the top quarks where the decay products of the W boson are contained within an AK8 jet. To fully reconstruct the hadronically decaying top quark, the AK8 jet corresponding to the W boson is combined with an AK4 jet satisfying additional top quark mass and cone size requirements.

To identify high-p_T top quarks, AK8 jets with jet p_T larger than 400 GeV are used. The mass of the jet is corrected with the soft-drop method [61, 62], using angular exponent $\beta = 0$, soft cutoff threshold $z_{\text{cut}} < 0.1$, and characteristic radius $R_0 = 0.8$. The soft-drop algorithm reclusters the AK8 jet into subjets, using the Cambridge-Aachen algorithm [63, 64], to remove soft radiation which can bias the jet mass. To be considered as a top candidate this soft-drop mass must fall within the range of 105 to 210 GeV. In addition, the N-subjettiness variables τ_N [65] are used

to determine how consistent the jet is with having a given number of subjets. The requirement placed here is that $\tau_3/\tau_2 < 0.65$. Full details on this algorithm can be found in Ref. [59]. To avoid overlap between these top-tagged AK8 jets (also denoted "monojet") and the AK4 jets that are used to reconstruct fully resolved ("trijet") or partially merged ("dijet") top quarks, all AK4 jets matched to the top-tagged AK8 jet are removed from the list of AK4 jets used in the reconstruction of the dijet and trijet categories. An AK4 jet is considered matched when it is within $\Delta R < 0.4$ of one of the soft-drop subjets of the tagged AK8 jet.

For the category of top quark decays where the two decay products of the W boson are merged into a single AK8 jet, we use similar techniques to identify the W jet. We require an AK8 jet to have $p_T > 200\,\text{GeV}$ and soft-drop corrected mass between 65 and 100 GeV. In order for the jet to be consistent with having two subjets, we require $\tau_2/\tau_1 < 0.6$. This W jet can then be combined with an AK4 jet with $p_T > 30\,\text{GeV}$ to form a top quark candidate. A valid top quark candidate for this dijet category should have a mass between 100 and 250 GeV, both jets should fall inside a cone of $\Delta R < 1$ of the sum-p_T vector, and the ratio of the soft-drop corrected mass of the W jet to the top quark candidate mass should be between $0.85(m_W/m_t)$ and $1.25(m_W/m_t)$, where $m_W = 80.385\,\text{GeV}$ and $m_t = 173.5\,\text{GeV}$. If more than one valid combination can be made using the same jet, the combination with total mass closest to the top quark mass is chosen. All AK4 jets corresponding to top candidates of this type are removed from the list that is passed along to the resolved top tagging algorithm. These AK4 jets are either AK4 jets matched to the soft-drop subjets of the W-tagged AK8 jet, or the AK4 jet that is combined with the W jet to form the top candidate.

In the resolved algorithm, trijet combinations of AK4 jets with $|\eta| < 5.0$ are used as candidates for top quark decays. Although this approach allows the reconstruction of top quark decays with much lower p_T, the method suffers from large combinatorial background from additional jets in the event. To address this two techniques are employed. The first is to limit the number of combinations which can be made. This is accomplished by requiring the individual jets to satisfy $p_T > 30\,\text{GeV}$, the three jets to lie within a cone of $\Delta R < 1.5$, and that there be no more than one b-tagged jet in the candidate. The second technique uses a random forest decision tree [66] to discriminate between top-like combinations and background. A random forest decision tree is constructed from an ensemble of traditional decision trees which are each trained on a different subset of the total training data. The individual trees are further differentiated from each other by limiting the number of variables which are considered at any branch node of the tree to a random subset of the total variables equal to the square root of the total number of variables. The final discriminator is then the mean decision from the entire ensemble. The random forest algorithm is used because it is resilient against overfitting while still maintaining good separation power because the individual trees can be kept much deeper than traditional decision trees.

The random forest is trained using a sample of 100 000 semi-leptonic $t\bar{t}$ and 70 000 $Z \to \nu\bar{\nu}$ simulated events. Signal events are defined from the $t\bar{t}$ simulation as any trijet combination for which all three jets are matched to the simulated generator-level top quark decay products with a cone of $\Delta R < 0.4$ and whose overall momentum vector is matched to the generator-level top quark with a cone of $\Delta R < 0.6$. This strict matching ensures that no background contaminates the signal sample. The background combinations are taken from both the $t\bar{t}$ sample and the $Z \to \nu\bar{\nu}$ sample from any trijet combination which has no jets matched to the generator-level top quark decay products. It is possible that there is more than one background combination in each event and all are used in the training.

The variables considered by the random forest algorithm include the mass of the trijet system,

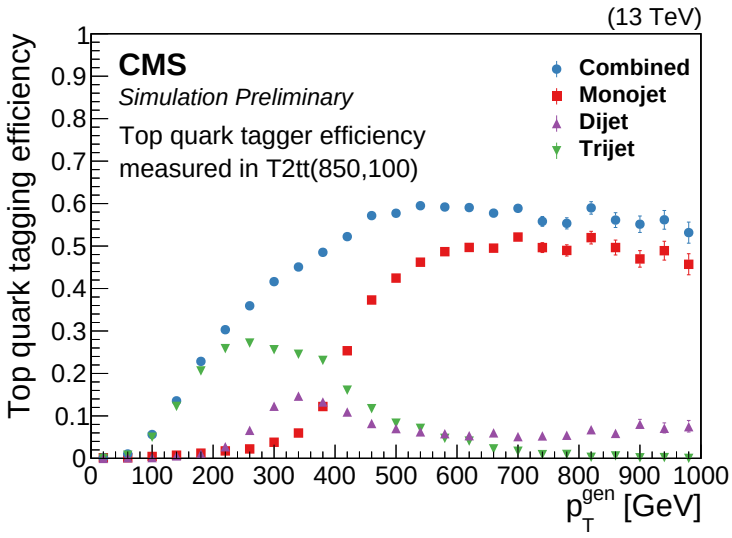

Figure 2: The tagging efficiency of the top quark tagger as a function of the generator-level hadronically decaying top quark p_T. The efficiencies of the monojet (red boxes), dijet (magenta upper-triangles), and trijet (green lower-triangles) categories are shown together with the efficiency of their combination (blue circles). The efficiency is computed using the T2tt signal model with $m_{\tilde{t}} = 850\,\text{GeV}$ and $m_{\tilde{\chi}_1^0} = 100\,\text{GeV}$, and it is similar for $t\bar{t}$ events. The vertical bars depict the statistical uncertainty.

the mass of each dijet combination, the angular separation and momentum of the jets in the trijet rest frame, the b tagging discriminator value for each jet, and the quark-gluon discriminator [67] value for each jet. To keep the random forest from overtraining on the p_T of the top candidate, special measures were taken to remove the candidate p_T and correlated variables. The signal and background events were weighted to flatten the p_T spectrum, and the kinematic variables in the lab frame were replaced with their equivalent variables in the rest frame of the trijet system. The jets are sorted by their momentum in the rest frame, because the leading momentum jet is most likely to originate from a b quark while the lowest momentum jet is almost never the b-tagged jet.

The list of resolved top quark candidates is obtained by selecting all trijet candidates with random forest discriminator value above 0.85. If any trijet combinations share one or more AK4 jets, the combination with the largest discriminator value is chosen, and the others are discarded.

The final list of all tagged top quarks encompasses the non-overlapping candidates from all three reconstruction techniques. The total efficiency of the top quark tagging algorithm, including a breakdown into the different categories, is shown in Fig. 2. The efficiency is measured using a T2tt(850, 100) signal sample based on the number of generator-level top quarks that are matched to a reconstructed top quark candidate divided by the total number of generator-level top quarks that decay hadronically. The matching between the generator-level top quarks and the reconstructed top quarks requires that the overall reconstructed top is matched to the generator-level top quark within $\Delta R < 0.4$. The fake rate is measured in $Z \to \nu\bar{\nu}$ MC requiring no electrons or muons with $p_T > 10$ GeV, $E_T^{miss} > 250$ GeV, at least four jets, and at least one b tagged jet and is found to be 20% on average.

4.2 Event selection

Events in the search regions are collected with a trigger that applies a lower threshold of 100 GeV on $E_{\mathrm{T}}^{\mathrm{miss}}$ in coincidence with a threshold of 100 GeV on the magnitude of the vector sum of all jet transverse momenta $H_{\mathrm{T}}^{\mathrm{miss}}$. This trigger is fully efficient at selecting events satisfying $E_{\mathrm{T}}^{\mathrm{miss}} > 250$ GeV at the full event reconstruction level.

All events must pass filters designed to remove detector- and beam-related noise. All jets considered in this analysis are required to have $p_{\mathrm{T}} > 30$ GeV, and must pass a set of jet identification criteria as described in Ref. [68]. The minimum number of such jets with $|\eta| < 2.4$ in an event must be $N_{\mathrm{j}} \geq 4$, with the leading two jets required to have $p_{\mathrm{T}} > 50$ GeV. Events must satisfy $E_{\mathrm{T}}^{\mathrm{miss}} > 250$ GeV and $H_{\mathrm{T}} > 300$ GeV. A requirement on the angle between $\vec{p}_{\mathrm{T}}^{\mathrm{miss}}$ and the first three leading jets, $\Delta\phi(\vec{p}_{\mathrm{T}}^{\mathrm{miss}}, j_{1,2,3}) > 0.5, 0.5, 0.3$, is applied to reduce the number of events from QCD multijet processes. High-$E_{\mathrm{T}}^{\mathrm{miss}}$ QCD multijet events are usually the result of an undermeasurement of the p_{T} of one of the leading jets, which results in $\vec{p}_{\mathrm{T}}^{\mathrm{miss}}$ being aligned with that jet and $\Delta\phi(\vec{p}_{\mathrm{T}}^{\mathrm{miss}}, j_{1,2,3})$ being small. The undermeasurement can occur because of detector effects or, in the case of semileptonic b or c quark decays, because a neutrino carries away unmeasured energy. Finally, requirements that $N_{\mathrm{t}} \geq 1$, $N_{\mathrm{b}} \geq 1$, and $M_{\mathrm{T2}} > 200$ GeV are applied, defining the analysis preselection.

The M_{T2} variable [22, 69, 70] is designed to estimate the transverse mass of pair produced heavy particles, here gluinos or top squarks, which both decay to both visible and invisible particles. The M_{T2} variable has a kinematic upper limit at the mass of the heavy particle produced. If the top quarks originate from pair production of top squarks, this limit will be much higher than if they originate from SM $\mathrm{t\bar{t}}$ production. If they originate from gluino decays there is no kinematic upper limit; however, the large $E_{\mathrm{T}}^{\mathrm{miss}}$ and high top quark p_{T} leads to large M_{T2} values for these models separating them from $\mathrm{t\bar{t}}$ production. In the case that there are two tagged top quarks, M_{T2} is calculated using the pair of tagged top quarks and $E_{\mathrm{T}}^{\mathrm{miss}}$. In case there are more than two tagged top candidates in the event, we compute M_{T2} for all combinations and choose the smallest M_{T2} value. If there is only one top candidate identified by the top tagging algorithm, we reconstruct a proxy for the other top quark by using the b-tagged jet as a seed. If no b-tagged jet is found, because the required b-tagged jet may be part of the reconstructed top quark, the highest p_{T} jet is used instead. The seed jet is combined with another AK4 jet if the combination has an invariant mass between 50 and 220 GeV and both jets are within $\Delta R = 1.5$ of each other. In this case, M_{T2} is calculated from the tagged top quark, the top quark proxy (either single seed jet, or seed jet combined with an extra jet), and $E_{\mathrm{T}}^{\mathrm{miss}}$.

The search region is divided into 84 non-overlapping regions in terms of N_{t}, N_{b}, $E_{\mathrm{T}}^{\mathrm{miss}}$, H_{T}, and M_{T2}. Search regions with $N_{\mathrm{b}} \leq 2$ and $N_{\mathrm{t}} \leq 2$ use $E_{\mathrm{T}}^{\mathrm{miss}}$ and M_{T2} as other binning dimensions, whereas bins with $N_{\mathrm{b}} \geq 3$ or $N_{\mathrm{t}} \geq 3$ use $E_{\mathrm{T}}^{\mathrm{miss}}$ and H_{T}, as can be seen in Fig. 3.

5 Background estimation

The largest source of SM background comes from $\mathrm{t\bar{t}}$, W+jets, and single top quark events with a leptonic W boson decay. These events account for about 75% integrated over all search bins. Leptonic events can pass the lepton vetoes in the event selection in two ways. If the W boson decays to a τ lepton that decays hadronically, this τ lepton is reconstructed as a jet. If, on the other hand, the W boson decays to an electron or muon, events can survive when the electron or muon is "lost", i.e., is not isolated, not identified/reconstructed, or out of the detector acceptance. These two sources of the background are often referred to as the hadronic-τ and lost-lepton backgrounds. The remaining SM background contributions originate from the

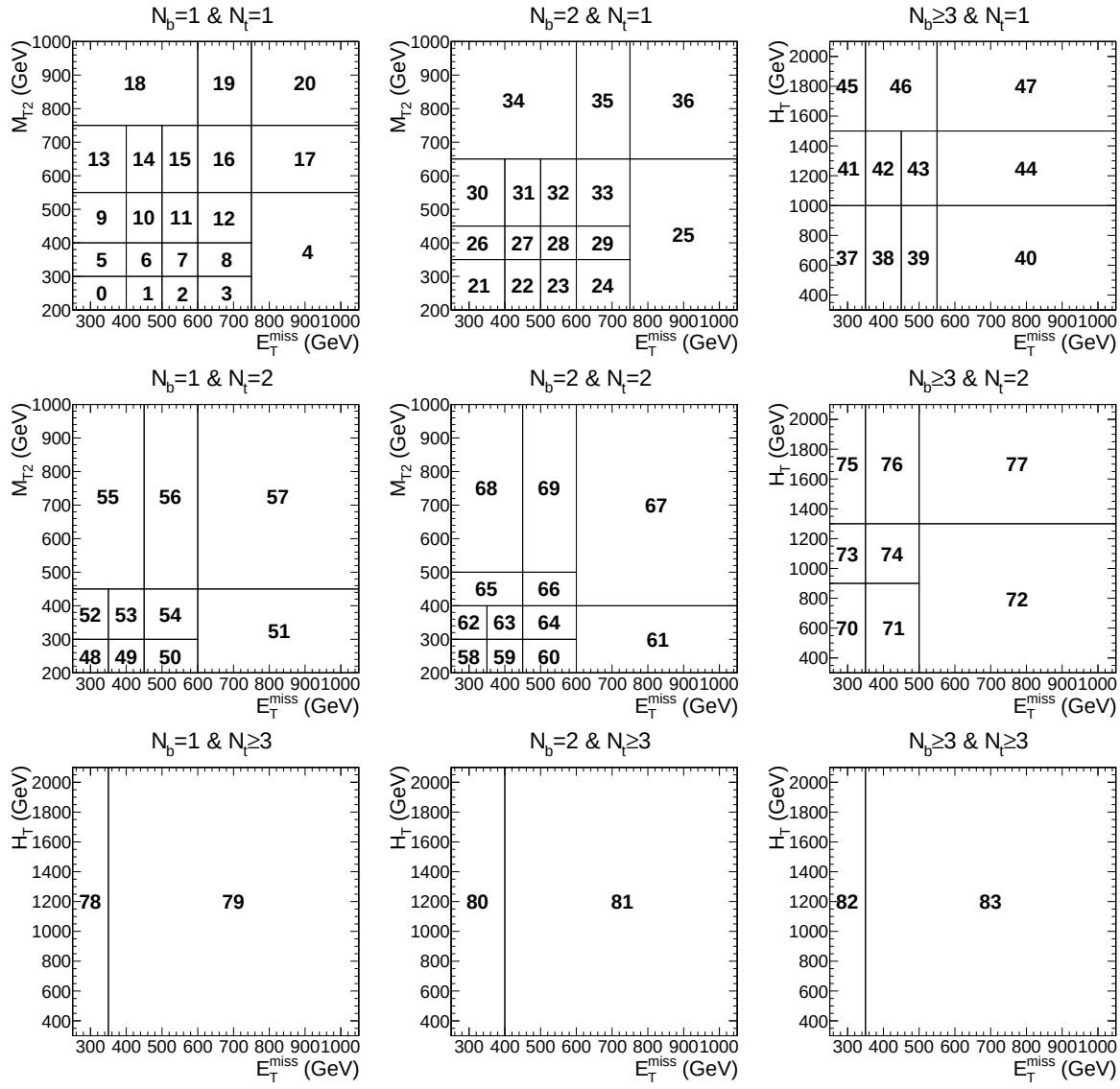

Figure 3: Search region definitions for bin numbers 0–83. The highest $E_{\mathrm{T}}^{\mathrm{miss}}$ and $M_{\mathrm{T2}}/H_{\mathrm{T}}$ bins are open-ended, e.g., bin 20 requires $E_{\mathrm{T}}^{\mathrm{miss}} > 750\,\mathrm{GeV}$ and $M_{\mathrm{T2}} > 750\,\mathrm{GeV}$.

$Z \to \nu\bar{\nu}$ +jets, which has genuine E_T^{miss}, QCD multijet, which can have substantial E_T^{miss} from jet mismeasurements, and rare processes such as $t\bar{t}Z$. The following sections will briefly discuss each of the background estimation methods, focusing on the differences w.r.t. the methods used in Ref. [22].

5.1 Background from leptonic W boson decays

The contribution to the background from leptonic W boson decays is determined from a data control sample (CS) that consists mainly of $t\bar{t}$ events. Events in this CS are collected using the same triggers as used for the signal region and must pass the preselection requirements, apart from the lepton (muon or electron) veto which is replaced by the requirement that there be exactly one identified and isolated muon or election candidate satisfying the lepton selection used in lepton vetoes. The isolated track veto is removed from the CS requirements as well. To reduce possible signal contamination in this CS, only events with m_T less than 100 GeV are considered, with m_T reconstructed from the lepton (muon or electron) p_T and E_T^{miss}.

The predicted number of background events with leptonic W boson decays from $t\bar{t}$, W+jets, and single top processes contributing to each search region bin is calculated as the sum over the events in the corresponding single-lepton CS in data multiplied by a translation factor. The translation factor is calculated for each search bin as the ratio of the number of simulated lost-lepton and hadronic-τ events in the search region bin to the number of simulated single muon or electron events in the corresponding CS bin. In order to measure the translation factor as close to data as possible, the simulated events are corrected for the modeling of the initial state radiation (ISR) jet spectrum, the b tagging efficiency scale factor and differences in the muon and electron identification and isolation cut efficiency between data and simulation.

The translation factor method is validated using an orthogonal data control sample selected by requiring $N_t = 0$. Additionally, $N_b \geq 2$ and $\Delta\phi(\vec{p}_T^{miss}, j_{1,2,3,4}) > 0.5$ are required to reduce the $Z \to \nu\bar{\nu}$ and/or the QCD contributions. This control sample is dominated by events from leptonic top quark decays. The background yield from leptonic W boson decays from $t\bar{t}$, W+jets, and single top is estimated using the translation factor method. Simulated event yields are used for all other processes. Fig. 4 shows that the predictions from the translation factor method agree well with observed data within statistical uncertainties across the entire E_T^{miss} spectrum.

The main systematic uncertainty in this background prediction is the statistical uncertainty in the translation factors. This uncertainty ranges between 1% and 40%. The following systematic uncertainties are also included: uncertainty in the lepton reconstruction and isolation efficiency (effect on prediction is between 7% and 43%), jet and E_T^{miss} energy scale and resolution uncertainties (up to 64%), uncertainties in the modeling of the ISR jet spectrum (up to 13%), uncertainties in the PDFs (up to 32%), and b tagging efficiency scale factor uncertainties (1%).

The lost-lepton component of this background is also estimated using a complementary method described in Ref. [22], which uses the same sample of single electron or muon events. In this approach, the lost-lepton background is estimated using factors that convert the number of events in the CS to the number of lost-lepton events due to isolation, reconstruction and identification, and acceptance criteria. These factors are determined from isolation and reconstruction efficiencies, as well as the acceptance, which are obtained for each search region bin using simulated $t\bar{t}$, W+jets, and single top quark events. The lost-lepton background yields obtained with this approach are consistent with those from the translation factors within uncertainties.

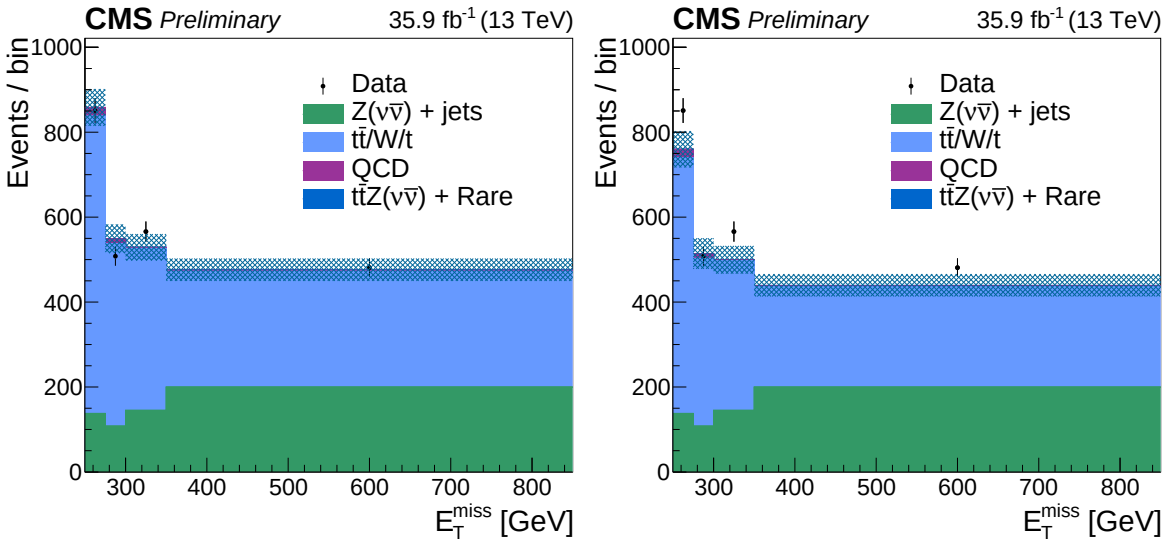

Figure 4: Validation of the translation factor method in the control sample selected by requiring $N_t = 0$ and $N_b \geq 2$ from the muon channel (left) and electron channel (right). The black points are observed data. The light blue histogram shows the prediction from $t\bar{t}$, W+jets, and single top events using the translation factor method. All other backgrounds come directly from simulated event yields. The shaded area includes only statistical uncertainties in the background estimate.

5.2 Background from $Z \to \nu\bar{\nu}$ events

The $Z \to \nu\bar{\nu}$ background is estimated using simulated events which are corrected for differences observed between data and simulation in a dimuon control sample. The dimuon control sample is selected using events with two opposite charge muons with $p_T > 50(20)$ GeV requirement for the leading(sub-leading) muon and an invariant mass between 81 GeV and 101 GeV. The events are then reconstructed as if the muons were neutrinos to simulate $Z \to \nu\bar{\nu}$ events.

The first set of correction factors adjusts for differences between the N_j distribution in data and simulation. This correction is derived in a loose control sample with the same requirements on $\Delta\phi(\vec{p}_T^{\,miss}, j_{1,2,3})$, H_T, and N_t as the signal region, but with $E_T^{miss} > 100$ GeV and no requirement on N_b. The correction factor is derived as a function of N_j by taking the ratio of data, with non-DY backgrounds subtracted, to the DY simulation. These correction factors are then applied to the $Z \to \nu\bar{\nu}$ simulation as weights based upon N_j in each event. The second correction factor adjusts the overall normalization between data and simulation. It is derived in a tight selection which matches the signal selection, except the muon and isolated track vetos are replaced with the dimuon selection and the N_b requirement is removed. This correction factor is derived by taking the ratio of the total number of events in data, with non-DY backgrounds subtracted, to that in the DY simulation.

The primary sources of systematic uncertainty for the $Z \to \nu\bar{\nu}$ background estimation are derived from the residual shape differences observed between data and simulation in the loose dimuon control sample as a function of the search region binning variables E_T^{miss}, M_{T2}, H_T, N_b, and N_t. This comparison between data and simulation can be seen for N_b and E_T^{miss} in Fig. 5. The shift in the central value between data and simulation leads to an uncertainty varying between 14% and 44% depending on the analysis bin. The statistical uncertainty on the N_j shape correction using the loose control sample (1% to 46%) and the overall normalization

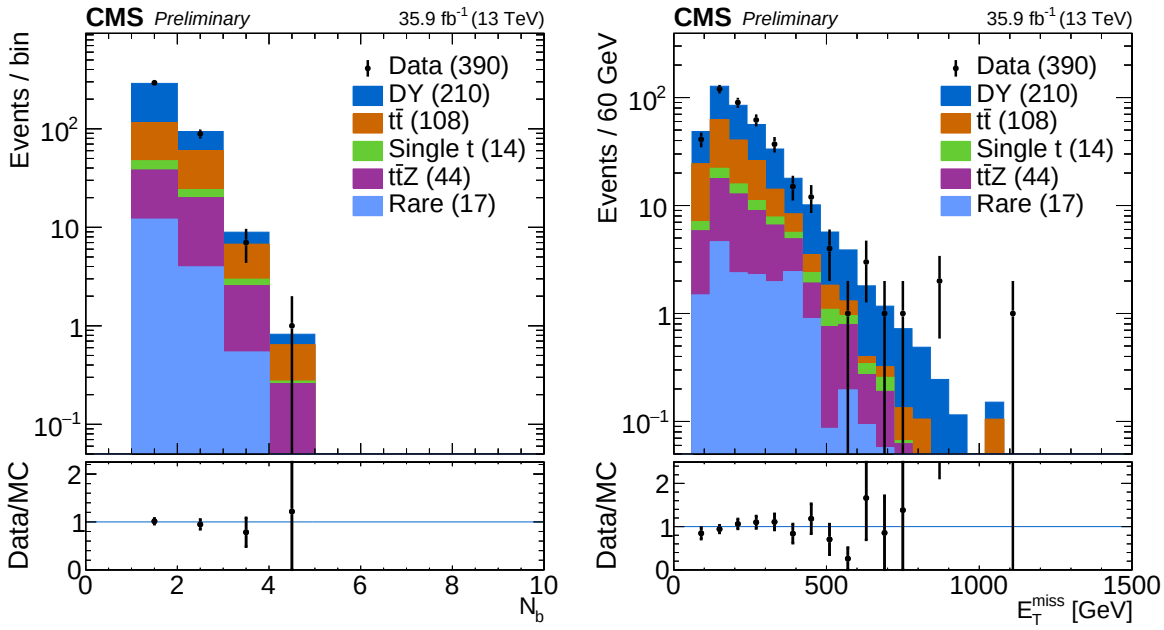

Figure 5: The N_b (left) and E_T^{miss} (right) distributions from data and simulation in the loose $Z \to \mu\mu$ control region, after applying the $S_{DY}(N_j)$ scale factor to the simulation. The lower panels show the ratio between data and simulation. Only statistical uncertainties are shown. The values in parentheses in the legend indicate the integrated yield for each given process.

using the tight control sample (7.9%) are also taken as a systematic uncertainties. Other systematic uncertainties include jet and E_T^{miss} energy scale uncertainties (1% to 71%), the b tagging efficiency scale factor uncertainties (1% to 23%), uncertainties in the PDFs and renormalization/factorization scale choices (1% to 48%), the statistical uncertainty from the total number of simulated events in each bin (1% to 81% with a few bins as high as 100%), and trigger efficiency uncertainties (less than 14%).

5.3 Background from multijet events

The background from QCD multijet events is estimated using a combination of data and simulation. A data control sample is defined using the same selection as defined in Section 4.2, but with the E_T^{miss} requirement reduced to 200 GeV and the selection on $\Delta\phi(\vec{p}_T^{miss}, j_{1,2,3})$ being inverted. This yields a signal-depleted control sample, which is predominantly QCD multijet events, though some contamination from other SM backgrounds is present. These are subtracted from the QCD control sample using background estimates made specifically in this region using the methods described in the previous sections. The yields from the QCD control sample for each search bin are extrapolated to the signal region using translation factors derived using simulated QCD multijet events as a function of E_T^{miss} and M_{T2}. The translation factors derived from simulation are normalized to data using the $200 < E_T^{miss} < 250$ GeV region of the QCD control sample.

A closure test is performed by comparing the prediction from simulation using the search selection with the prediction derived from the inverted $\Delta\phi$ selection by applying the data-normalized translation factors. Any non-closure is applied as a systematic uncertainty to the final event yields in each search bin (30% to 500%). Another large source of uncertainty comes from the statistical uncertainty in the translation factors (30% to 300%). The final significant source of uncertainty in the QCD multijet prediction arises from the subtraction of non-QCD backgrounds from the QCD control sample (2% to 50%).

5.4 Background from rare processes

Background contributions from sources other than $t\bar{t}$, W+jets, and $Z \to \nu\bar{\nu}$ form only a small fraction of the total background. These have only a small effect on the final result and so their estimates are taken directly from simulation. Among these additional sources of background the largest contribution is from $t\bar{t}Z$ production. A comparison is done in the three-lepton control sample to check the overall cross section of the $t\bar{t}Z$ simulation. The data and MC agree within the statistical uncertainty of 30%, which is taken as a systematic uncertainty in the $t\bar{t}Z$ background estimation.

6 Results and interpretation

The predicted number of SM background events and the number of events observed in data for each of the search regions defined in Secion 4.2 are summarized in Fig. 6 and Tables 1 and 2. Typically, the most significant background across the search regions comes from SM $t\bar{t}$ or W boson production, where the W boson decay contains genuine $E_{\mathrm{T}}^{\mathrm{miss}}$ from a neutrino. Generally, the next largest contribution comes from $Z \to \nu\bar{\nu}$ production in association with jets (including heavy-flavor jets) in which the neutrino pair gives rise to large $E_{\mathrm{T}}^{\mathrm{miss}}$ and the top quark conditions are satisfied by an accidental combination of the jets. For search regions with very high $E_{\mathrm{T}}^{\mathrm{miss}}$ requirements, the $Z \to \nu\bar{\nu}$ background can become dominant. The QCD multijet contribution and the contribution from other rare SM processes are subdominant across all bins. The largest rare SM process contribution (though still small) comes from $t\bar{t}Z$ with the Z boson decaying into a pair of neutrinos. No statistically significant deviation between the observed data events and the SM background prediction is found.

The statistical interpretation of the results in terms of exclusion limits for the signal models considered is based on a binned likelihood fit to the observed data, taking into account the predicted background and expected signal yields with their uncertainties in each bin. The extraction of exclusion limits is based on a modified frequentist approach [71–74] using a profile likelihood ratio as the test statistic. Signal models for which the 95% confidence level (CL) upper limit on the production cross section falls below the theoretical cross section (based on NLO+NLL calculations [51]) are considered to be excluded by the analysis.

The uncertainties in the signal modeling are determined per search region bin and include the following sources: simulation sample size, luminosity determination (2.6%), lepton and isolated track veto (up to 6.8%), b tagging efficiency corrections used to scale simulation to data (up to 21%), trigger efficiency (up to 2.6%), renormalization and factorization scale variations (up to 3.5%), initial-state radiation (up to 46%), jet energy scale corrections (up to 34%), top quark reconstruction efficiency difference between data and full simulation (up to 14%), and the modeling of the fast simulation compared with the full simulation for top quark reconstruction and mistagging (up to 24%). All these uncertainties, apart from those arising from the simulation sample size, are treated as fully correlated between the search bins when computing exclusion limits. Potential contamination of signal events in the single-lepton control regions is taken into account for each signal model considered in the interpretation. The potential contamination in the dilepton and inverted-$\Delta\phi$ region is negligible.

Figure 7 shows 95% CL exclusion limits obtained for simplified models in the T2tt scenario. As a result of this analysis, top squark masses up to 1020 GeV and LSP masses up to 430 GeV are excluded. Figure 8 shows 95% CL exclusion limits obtained for simplified models in the T1tttt and T5ttcc scenarios. Gluino masses up to 2040 GeV and LSP masses up to 1150 GeV are excluded for T1tttt simplified models. For the T5ttcc simplified models, gluino masses up

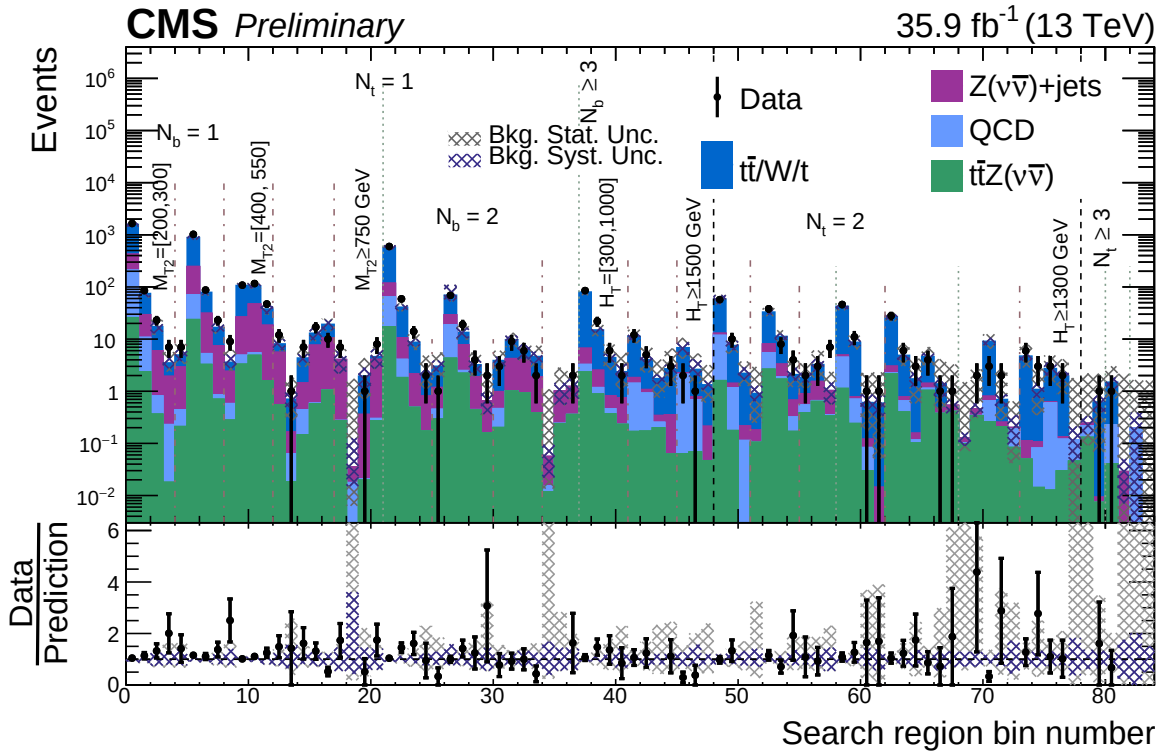

Figure 6: Observed event yields in data (black points) and predicted SM background (filled solid area) for the 84 search bins. The lower panel shows the ratio of data over total background prediction in each search bin. For both panels, the error bars show the statistical uncertainty associated with the observed data counts, and the grey (blue) hatched bands indicate the statistical (systematic) uncertainties in the total predicted background.

Table 1: The observed yields from data compared to the total background predictions for the first 48 search bins. The quoted uncertainties on the predicted background yields are statistical and systematic, respectively.

Search Bin	N_t	N_b	M_{T2} [GeV]	E_T^{miss} [GeV]	Data	Predicted background
0	1	1	200-300	250-400	1649	$1580^{+30}_{-30}{}^{+130}_{-140}$
1	1	1	200-300	400-500	85	$75^{+7}_{-6}{}^{+10}_{-10}$
2	1	1	200-300	500-600	23	$17^{+4}_{-3}{}^{+4}_{-4}$
3	1	1	200-300	600-750	7	$3.5^{+1.8}_{-0.8}{}^{+1.1}_{-0.7}$
4	1	1	200-550	750+	7	$5.0^{+2.4}_{-1.1}{}^{+2.0}_{-1.2}$
5	1	1	300-400	250-400	1020	$880^{+20}_{-20}{}^{+80}_{-80}$
6	1	1	300-400	400-500	87	$79^{+7}_{-6}{}^{+9}_{-9}$
7	1	1	300-400	500-600	23	$17^{+4}_{-2}{}^{+3}_{-3}$
8	1	1	300-400	600-750	9	$3.6^{+2.1}_{-0.8}{}^{+1.4}_{-0.8}$
9	1	1	400-550	250-400	108	$106^{+8}_{-7}{}^{+10}_{-10}$
10	1	1	400-550	400-500	116	$105^{+7}_{-6}{}^{+10}_{-10}$
11	1	1	400-550	500-600	47	$38^{+5}_{-4}{}^{+7}_{-7}$
12	1	1	400-550	600-750	12	$8.1^{+2.4}_{-1.2}{}^{+1.9}_{-1.9}$
13	1	1	550-750	250-400	1	$0.7^{+1.0}_{-0.3}{}^{+0.4}_{-0.2}$
14	1	1	550-750	400-500	7	$4.3^{+2.0}_{-1.1}{}^{+0.8}_{-0.8}$
15	1	1	550-750	500-600	17	$13^{+3}_{-2}{}^{+3}_{-3}$
16	1	1	550-750	600-750	10	$19^{+3}_{-2}{}^{+4}_{-4}$
17	1	1	550-750	750+	7	$4.0^{+1.5}_{-0.3}{}^{+1.8}_{-1.8}$
18	1	1	750+	250-600	0	$0.04^{+1.68}_{-0.02}{}^{+0.09}_{-0.02}$
19	1	1	750+	600-750	1	$1.9^{+2.2}_{-1.0}{}^{+0.9}_{-0.8}$
20	1	1	750+	750+	8	$4.6^{+1.6}_{-0.5}{}^{+1.9}_{-1.9}$
21	1	2	200-350	250-400	596	$570^{+20}_{-20}{}^{+50}_{-50}$
22	1	2	200-350	400-500	59	$41^{+6}_{-5}{}^{+5}_{-5}$
23	1	2	200-350	500-600	14	$8.7^{+3.4}_{-2.1}{}^{+1.3}_{-1.3}$
24	1	2	200-350	600-750	2	$2.1^{+2.7}_{-0.8}{}^{+0.5}_{-0.5}$
25	1	2	200-650	750+	1	$3.0^{+2.4}_{-1.0}{}^{+0.9}_{-0.6}$
26	1	2	350-450	250-400	69	$69^{+6}_{-5}{}^{+40}_{-16}$
27	1	2	350-450	400-500	19	$13^{+4}_{-2}{}^{+3}_{-3}$
28	1	2	350-450	500-600	4	$3.2^{+2.1}_{-0.9}{}^{+1.0}_{-1.0}$
29	1	2	350-450	600-750	2	$0.6^{+1.4}_{-0.1}{}^{+0.3}_{-0.3}$
30	1	2	450-650	250-400	3	$3.9^{+2.0}_{-1.1}{}^{+0.7}_{-0.8}$
31	1	2	450-650	400-500	9	$9.7^{+2.7}_{-1.8}{}^{+2.1}_{-2.0}$
32	1	2	450-650	500-600	6	$6.0^{+1.6}_{-0.9}{}^{+1.9}_{-1.9}$
33	1	2	450-650	600-750	2	$4.6^{+2.6}_{-1.3}{}^{+1.2}_{-1.2}$
34	1	2	650+	250-600	0	$0.06^{+1.03}_{-0.03}{}^{+0.04}_{-0.03}$
35	1	2	650+	600-750	0	$1.0^{+1.8}_{-0.1}{}^{+0.5}_{-0.5}$
36	1	2	650+	750+	2	$1.2^{+1.1}_{-0.1}{}^{+0.5}_{-0.5}$
37	1	3+	300-1000	250-350	85	$80^{+9}_{-8}{}^{+7}_{-7}$
38	1	3+	300-1000	350-450	22	$15^{+5}_{-3}{}^{+2}_{-2}$
39	1	3+	300-1000	450-550	6	$4.4^{+3.4}_{-1.7}{}^{+0.8}_{-0.8}$
40	1	3+	300-1000	550+	2	$2.4^{+2.9}_{-1.0}{}^{+1.0}_{-0.7}$
41	1	3+	1000-1500	250-350	12	$11^{+4}_{-2}{}^{+2}_{-2}$
42	1	3+	1000-1500	350-450	5	$4.0^{+2.6}_{-1.5}{}^{+0.9}_{-0.9}$
43	1	3+	1000-1500	450-550	0	$1.7^{+2.3}_{-0.9}{}^{+0.4}_{-0.4}$
44	1	3+	1000-1500	550+	3	$2.7^{+3.9}_{-1.4}{}^{+0.6}_{-0.5}$
45	1	3+	1500+	250-350	2	$6.8^{+3.2}_{-1.9}{}^{+1.8}_{-1.8}$
46	1	3+	1500+	350-550	1	$2.6^{+2.2}_{-1.0}{}^{+1.5}_{-0.7}$
47	1	3+	1500+	550+	0	$1.3^{+1.8}_{-0.7}{}^{+0.3}_{-0.3}$

Table 2: The observed yields from data compared to the total background predictions for the remaining search bins. The quoted uncertainties on the predicted background yields are statistical and systematic, respectively.

Search Bin	N_t	N_b	M_{T2} [GeV]	E_T^{miss} [GeV]	Data	Predicted background
48	2	1	200-300	250-350	57	$58^{+6}_{-5}{}^{+11}_{-11}$
49	2	1	200-300	350-450	10	$7.5^{+2.5}_{-1.7}{}^{+1.7}_{-1.4}$
50	2	1	200-300	450-600	0	$2.2^{+1.4}_{-0.8}{}^{+0.7}_{-0.5}$
51	2	1	200-450	600+	0	$0.9^{+2.0}_{-0.6}{}^{+0.4}_{-0.3}$
52	2	1	300-450	250-350	38	$33^{+5}_{-4}{}^{+3}_{-4}$
53	2	1	300-450	350-450	8	$11^{+3}_{-2}{}^{+2}_{-2}$
54	2	1	300-450	450-600	4	$2.1^{+1.7}_{-0.7}{}^{+0.7}_{-0.5}$
55	2	1	450+	250-450	2	$1.8^{+1.5}_{-0.6}{}^{+0.4}_{-0.4}$
56	2	1	450+	450-600	3	$3.2^{+2.7}_{-1.1}{}^{+0.9}_{-0.9}$
57	2	1	450+	600+	7	$1.0^{+1.2}_{-0.1}{}^{+0.5}_{-0.5}$
58	2	2	200-300	250-350	46	$42^{+5}_{-4}{}^{+5}_{-5}$
59	2	2	200-300	350-450	11	$8.7^{+2.7}_{-1.9}{}^{+1.4}_{-1.3}$
60	2	2	200-300	450-600	1	$0.6^{+1.6}_{-0.4}{}^{+0.3}_{-0.1}$
61	2	2	200-400	600+	1	$0.6^{+1.7}_{-0.5}{}^{+0.2}_{-0.2}$
62	2	2	300-400	250-350	28	$27^{+5}_{-4}{}^{+3}_{-3}$
63	2	2	300-400	350-450	6	$4.9^{+2.9}_{-1.6}{}^{+0.9}_{-0.9}$
64	2	2	300-400	450-600	3	$1.7^{+2.4}_{-1.0}{}^{+0.6}_{-0.5}$
65	2	2	400-500	250-450	4	$4.6^{+2.3}_{-1.2}{}^{+0.7}_{-0.8}$
66	2	2	400-500	450-600	1	$1.4^{+2.7}_{-0.7}{}^{+0.4}_{-0.6}$
67	2	2	400+	600+	1	$0.5^{+2.7}_{-0.1}{}^{+0.2}_{-0.7}$
68	2	2	500+	250-450	0	$0.13^{+1.37}_{-0.04}{}^{+0.04}_{-0.04}$
69	2	2	500+	450-600	2	$0.5^{+2.2}_{-0.1}{}^{+0.2}_{-0.2}$
70	2	3+	300-900	250-350	3	$9.1^{+3.0}_{-2.0}{}^{+1.5}_{-1.4}$
71	2	3+	300-900	350-500	2	$0.7^{+1.9}_{-0.4}{}^{+0.2}_{-0.2}$
72	2	3+	300-1300	500+	0	$0.2^{+0.4}_{-0.1}{}^{+0.1}_{-0.1}$
73	2	3+	900-1300	250-350	6	$4.7^{+2.9}_{-1.7}{}^{+0.7}_{-0.9}$
74	2	3+	900-1300	350-500	3	$1.1^{+1.6}_{-0.6}{}^{+0.3}_{-0.3}$
75	2	3+	1300+	250-350	3	$2.7^{+2.0}_{-1.0}{}^{+0.8}_{-0.7}$
76	2	3+	1300+	350-500	2	$2.0^{+2.1}_{-1.0}{}^{+0.4}_{-0.4}$
77	2	3+	1300+	500+	0	$0.1^{+1.7}_{-0.1}{}^{+0.1}_{-0.1}$
78	3+	1	300+	250-350	0	$0.2^{+2.0}_{-0.2}{}^{+0.1}_{-0.1}$
79	3+	1	300+	350+	1	$0.6^{+1.5}_{-0.5}{}^{+0.2}_{-0.2}$
80	3+	2	300+	250-400	1	$1.5^{+1.5}_{-0.7}{}^{+0.4}_{-0.4}$
81	3+	2	300+	400+	0	$0.03^{+2.12}_{-0.03}{}^{+0.02}_{-0.02}$
82	3+	3+	300+	250-350	0	$0.2^{+1.4}_{-0.2}{}^{+0.2}_{-0.2}$
83	3+	3+	300+	350+	0	$0^{+1.6}_{-0}{}^{+0}_{-0}$

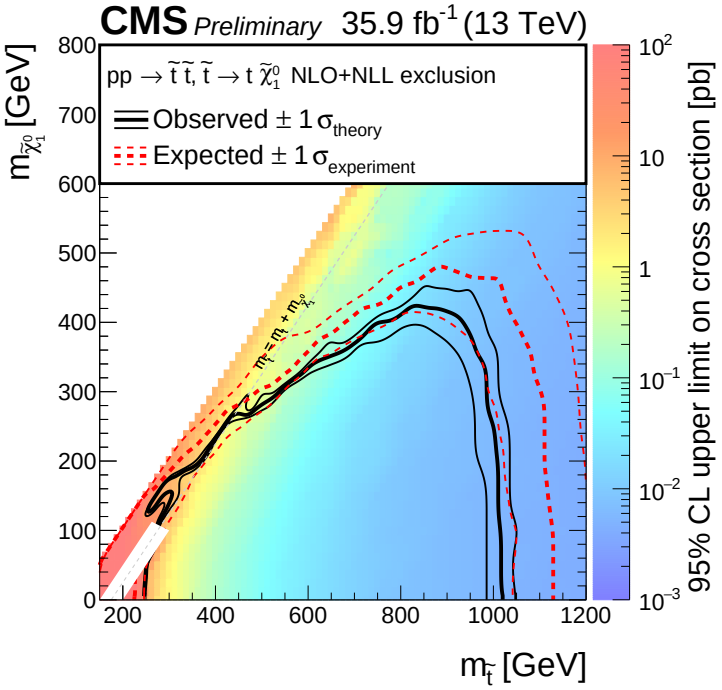

Figure 7: Exclusion limit at 95% CL for the simplified model of direct top squark pair production with $\tilde{t} \to t\tilde{\chi}_1^0$ decays (T2tt model). The solid black curves represent the observed exclusion contour with respect to NLO+NLL signal cross section calculations [51] and the corresponding ± 1 standard deviation uncertainties. The dashed red curves indicate the expected exclusion contour and the ± 1 standard deviation uncertainties including experimental uncertainties. No interpretation is provided for signal models for which $|m_{\tilde{t}} - m_{\tilde{\chi}_1^0} - m_t| \leq 25\,\text{GeV}$ and $m_{\tilde{t}} \leq 275\,\text{GeV}$ because of significant differences between the fast simulation and the GEANT4-based simulation for these low-E_T^{miss} scenarios.

to 1810 GeV and LSP masses up to 1100 GeV are excluded. These results significantly extend the mass reach compared to previous analyses at 13 TeV, which excluded gluino masses up to about 1780 GeV and LSP masses up to about 1020 GeV for the T1tttt model.

7 Summary

Results have been presented from a search for direct and gluino-mediated top squark production in final states that include tagged top quark decays. The search uses all-hadronic events with at least four jets and a large imbalance in transverse momentum (E_T^{miss}), selected from data corresponding to an integrated luminosity of 35.9 fb^{-1} collected in proton-proton collisions at a center-of-mass energy of 13 TeV with the CMS detector. A set of search regions is defined based on E_T^{miss}, M_{T2}, H_T, the number of top quark tagged objects, and the number of b-tagged jets. No statistically significant excess of events is observed above the expected standard model background. Exclusion limits are set at 95% confidence level for simplified models of direct top squark pair production and of gluino pair production, where the gluinos decay to final states that include top quarks. For simplified models of pair production of top squarks, which decay to a top quark and a neutralino, top squark masses up to 1020 GeV and neutralino masses up to 430 GeV are excluded at 95% confidence level. For simplified models of gluino pair production, gluino masses up to 2040 GeV and neutralino masses up to 1150 GeV are excluded for T1tttt models. For T5ttcc models, gluino masses up to 1810 GeV and neutralino masses up to 1100

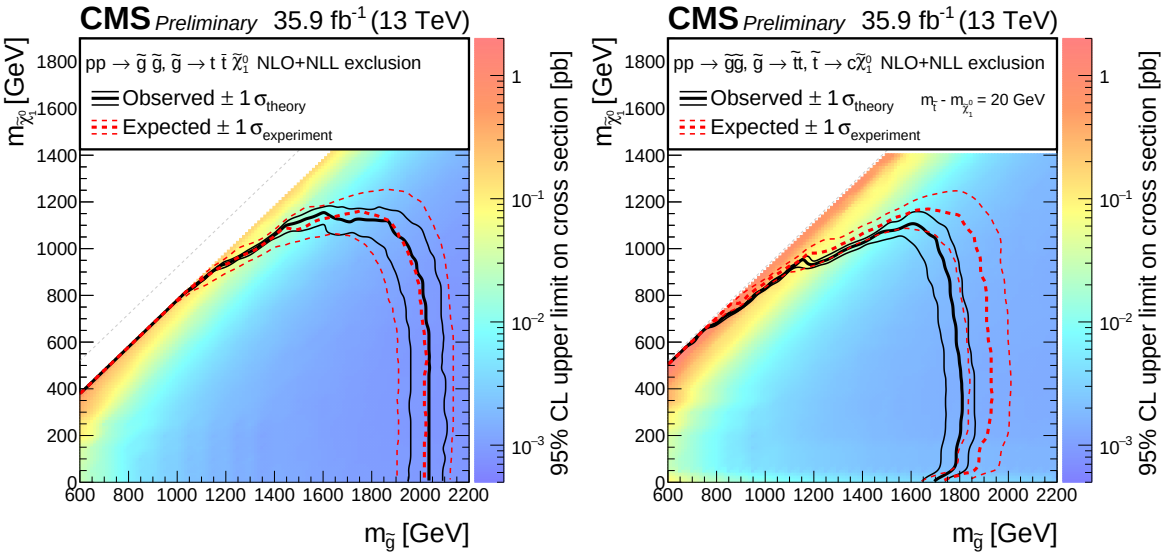

Figure 8: Exclusion limit at 95% CL for the simplified model of top squarks produced via decays of gluino pairs in the T1tttt (left) and T5ttcc (right) scenarios. The solid black curves represent the observed exclusion contour with respect to NLO+NLL signal cross section calculations [51] and the corresponding ± 1 standard deviation uncertainties. The dashed red curves indicate the expected exclusion contour and the ± 1 standard deviation uncertainties including experimental uncertainties.

GeV are excluded.

References

[1] ATLAS Collaboration, "Observation of a new particle in the search for the Standard Model Higgs boson with the ATLAS detector at the LHC", *Phys. Lett. B* **716** (2012) 1, doi:10.1016/j.physletb.2012.08.020, arXiv:1207.7214.

[2] CMS Collaboration, "Observation of a new boson at a mass of 125 GeV with the CMS experiment at the LHC", *Phys. Lett. B* **716** (2012) 30, doi:10.1016/j.physletb.2012.08.021, arXiv:1207.7235.

[3] CMS Collaboration, "Observation of a new boson with mass near 125 GeV in pp collisions at $\sqrt{s}$ = 7 and 8 TeV", *JHEP* **06** (2013) 081, doi:10.1007/JHEP06(2013)081, arXiv:1303.4571.

[4] L. Evans and P. Bryant, "LHC Machine", *JINST* **3** (2008) S08001, doi:10.1088/1748-0221/3/08/S08001.

[5] ATLAS and CMS Collaborations, "Combined Measurement of the Higgs Boson Mass in pp Collisions at $\sqrt{s} = 7$ and 8 TeV with the ATLAS and CMS Experiments", *Phys. Rev. Lett.* **114** (2015) 191803, doi:10.1103/PhysRevLett.114.191803, arXiv:1503.07589.

[6] R. Barbieri, S. Ferrara, and C. A. Savoy, "Gauge Models with Spontaneously Broken Local Supersymmetry", *Phys. Lett. B* **119** (1982) 343, doi:10.1016/0370-2693(82)90685-2.

[7] J. Wess and B. Zumino, "Supergauge transformations in four-dimensions", *Nucl. Phys. B* **70** (1974) 39, doi:10.1016/0550-3213(74)90355-1.

[8] Y. A. Gol'fand and E. P. Likhtman, "Extension of the algebra of Poincaré group generators and violation of P invariance", *JETP Lett.* **13** (1971) 323.

[9] D. V. Volkov and V. P. Akulov, "Possible universal neutrino interaction", *JETP Lett.* **16** (1972) 438.

[10] A. H. Chamseddine, R. L. Arnowitt, and P. Nath, "Locally supersymmetric grand unification", *Phys. Rev. Lett.* **49** (1982) 970, doi:10.1103/PhysRevLett.49.970.

[11] G. L. Kane, C. F. Kolda, L. Roszkowski, and J. D. Wells, "Study of constrained minimal supersymmetry", *Phys. Rev. D* **49** (1994) 6173, doi:10.1103/PhysRevD.49.6173, arXiv:hep-ph/9312272.

[12] P. Fayet, "Supergauge invariant extension of the Higgs mechanism and a model for the electron and its neutrino", *Nucl. Phys. B* **90** (1975) 104, doi:10.1016/0550-3213(75)90636-7.

[13] L. J. Hall, J. D. Lykken, and S. Weinberg, "Supergravity as the messenger of supersymmetry breaking", *Phys. Rev. D* **27** (1983) 2359, doi:10.1103/PhysRevD.27.2359.

[14] P. Ramond, "Dual theory for free fermions", *Phys. Rev. D* **3** (1971) 2415, doi:10.1103/PhysRevD.3.2415.

[15] M. Papucci, J. T. Ruderman, and A. Weiler, "Natural SUSY Endures", *JHEP* **09** (2012) 035, doi:10.1007/JHEP09(2012)035, arXiv:1110.6926.

[16] J. Alwall, P. Schuster, and N. Toro, "Simplified Models for a First Characterization of New Physics at the LHC", *Phys. Rev. D* **79** (2009) 075020, doi:10.1103/PhysRevD.79.075020, arXiv:0810.3921.

[17] J. Alwall, M.-P. Le, M. Lisanti, and J. G. Wacker, "Model-Independent Jets plus Missing Energy Searches", *Phys. Rev. D* **79** (2009) 015005, doi:10.1103/PhysRevD.79.015005, arXiv:0809.3264.

[18] LHC New Physics Working Group Collaboration, "Simplified Models for LHC New Physics Searches", *J. Phys. G* **39** (2012) 105005, doi:10.1088/0954-3899/39/10/105005, arXiv:1105.2838.

[19] D. Alves, E. Izaguirre, and J. G. Wacker, "Where the sidewalk ends: jets and missing energy search strategies for the 7 TeV LHC", *JHEP* **10** (2011) 012, doi:10.1007/JHEP10(2011)012, arXiv:1102.5338.

[20] CMS Collaboration, "Interpretation of searches for supersymmetry with simplified models", *Phys. Rev. D* **88** (2013) 052017, doi:10.1103/PhysRevD.88.052017, arXiv:1301.2175.

[21] CMS Collaboration, "Searches for pair production for third-generation squarks in $\sqrt{(s)} = 13$ TeV pp collisions", arXiv:1612.03877. Submitted to *Eur. Phys. J. C*.

[22] CMS Collaboration, "Search for supersymmetry in the all-hadronic final state using top quark tagging in pp collisions at $\sqrt{s}$ = 13 TeV", arXiv:1701.01954. Submitted to *Phys. Rev. D*.

[23] CMS Collaboration, "Search for new physics with the M_{T2} variable in all-jets final states produced in pp collisions at $\sqrt{s} = 13$ TeV", *JHEP* **10** (2016) 006, doi:10.1007/JHEP10(2016)006, arXiv:1603.04053.

[24] ATLAS Collaboration, "Search for top squarks in final states with one isolated lepton, jets, and missing transverse momentum in $\sqrt{s} = 13$ TeV pp collisions with the ATLAS detector", *Phys. Rev. D* **94** (2016) 052009, doi:10.1103/PhysRevD.94.052009, arXiv:1606.03903.

[25] CMS Collaboration, "Search for supersymmetry in events with one lepton and multiple jets in proton-proton collisions at $\sqrt{s} = 13$ TeV", *Phys. Rev. D* **95** (2017) 012011, doi:10.1103/PhysRevD.95.012011, arXiv:1609.09386.

[26] CMS Collaboration, "Search for supersymmetry in pp collisions at $\sqrt{s} = 13$ TeV in the single-lepton final state using the sum of masses of large-radius jets", *JHEP* **08** (2016) 122, doi:10.1007/JHEP08(2016)122, arXiv:1605.04608.

[27] CMS Collaboration, "Search for new physics in same-sign dilepton events in protonproton collisions at $\sqrt{s} = 13$ TeV", *Eur. Phys. J. C* **76** (2016) 439, doi:10.1140/epjc/s10052-016-4261-z, arXiv:1605.03171.

[28] CMS Collaboration, "Search for supersymmetry in the multijet and missing transverse momentum final state in pp collisions at 13 TeV", *Phys. Lett. B* **758** (2016) 152, doi:10.1016/j.physletb.2016.05.002, arXiv:1602.06581.

[29] ATLAS Collaboration, "Search for pair production of gluinos decaying via stop and sbottom in events with b-jets and large missing transverse momentum in pp collisions at $\sqrt{s} = 13$ TeV with the ATLAS detector", *Phys. Rev. D* **94** (2016) 032003, doi:10.1103/PhysRevD.94.032003, arXiv:1605.09318.

[30] ATLAS Collaboration, "Search for supersymmetry at $\sqrt{s} = 13$ TeV in final states with jets and two same-sign leptons or three leptons with the ATLAS detector", *Eur. Phys. J. C* **76** (2016) 259, doi:10.1140/epjc/s10052-016-4095-8, arXiv:1602.09058.

[31] CMS Collaboration, "The CMS experiment at the CERN LHC", *JINST* **3** (2008) S08004, doi:10.1088/1748-0221/3/08/S08004.

[32] CMS Collaboration, "Particle-Flow Event Reconstruction in CMS and Performance for Jets, Taus, and $E_{\mathrm{T}}^{\mathrm{miss}}$", CMS Physics Analysis Summary CMS-PAS-PFT-09-001, 2009.

[33] CMS Collaboration, "Commissioning of the Particle-flow Event Reconstruction with the first LHC collisions recorded in the CMS detector", CMS Physics Analysis Summary CMS-PAS-PFT-10-001, 2010.

[34] M. Cacciari, G. P. Salam, and G. Soyez, "The anti-k_t jet clustering algorithm", *JHEP* **04** (2008) 063, doi:10.1088/1126-6708/2008/04/063, arXiv:0802.1189.

[35] M. Cacciari and G. P. Salam, "Pileup subtraction using jet areas", *Phys. Lett. B* **659** (2007) 119, doi:10.1016/j.physletb.2007.09.077, arXiv:0707.1378.

[36] M. Cacciari, G. P. Salam, and G. Soyez, "FastJet user manual", *Eur. Phys. J. C* **72** (2012) 1896, doi:10.1140/epjc/s10052-012-1896-2, arXiv:1111.6097.

[37] CMS Collaboration, "Jet energy scale and resolution in the CMS experiment in pp collisions at 8 TeV", *JINST* **12** (2017) P02014, doi:10.1088/1748-0221/12/02/P02014, arXiv:1607.03663.

[38] CMS Collaboration, "Performance of b tagging at $\sqrt{s} = 8$ TeV in multijet, $\mathrm{t\bar{t}}$ and boosted topology events", CMS Physics Analysis Summary CMS-PAS-BTV-13-001, 2013.

[39] CMS Collaboration, "Identification of b quark jets at the CMS Experiment in the LHC Run 2", CMS Physics Analysis Summary CMS-PAS-BTV-15-001, 2016.

[40] D. Bertolini, P. Harris, M. Low, and N. Tran, "Pileup Per Particle Identification", *JHEP* **10** (2014) 059, doi:10.1007/JHEP10(2014)059, arXiv:1407.6013.

[41] J. Alwall et al., "The automated computation of tree-level and next-to-leading order differential cross sections, and their matching to parton shower simulations", *JHEP* **07** (2014) 079, doi:10.1007/JHEP07(2014)079, arXiv:1405.0301.

[42] NNPDF Collaboration, "Parton distributions for the LHC Run II", *JHEP* **04** (2015) 040, doi:10.1007/JHEP04(2015)040, arXiv:1410.8849.

[43] P. Nason, "A new method for combining NLO QCD with shower Monte Carlo algorithms", *JHEP* **11** (2004) 040, doi:10.1088/1126-6708/2004/11/040, arXiv:hep-ph/0409146.

[44] S. Frixione, P. Nason, and C. Oleari, "Matching NLO QCD computations with Parton Shower simulations: the POWHEG method", *JHEP* **11** (2007) 070, doi:10.1088/1126-6708/2007/11/070, arXiv:0709.2092.

[45] S. Alioli, P. Nason, C. Oleari, and E. Re, "A general framework for implementing NLO calculations in shower Monte Carlo programs: the POWHEG BOX", *JHEP* **06** (2010) 043, doi:10.1007/JHEP06(2010)043, arXiv:1002.2581.

[46] E. Re, "Single-top Wt-channel production matched with parton showers using the POWHEG method", *Eur. Phys. J. C* **71** (2011) 1547, doi:10.1140/epjc/s10052-011-1547-z, arXiv:1009.2450.

[47] T. Sjöstrand, S. Mrenna, and P. Z. Skands, "A Brief Introduction to PYTHIA 8.1", *Comput. Phys. Commun.* **178** (2008) 852, doi:10.1016/j.cpc.2008.01.036, arXiv:0710.3820.

[48] CMS Collaboration, "Event generator tunes obtained from underlying event and multiparton scattering measurements", *Eur. Phys. J. C* **76** (2016) 155, doi:10.1140/epjc/s10052-016-3988-x, arXiv:1512.00815.

[49] GEANT4 Collaboration, "GEANT4—a simulation toolkit", *Nucl. Instrum. Meth. A* **506** (2003) 250, doi:10.1016/S0168-9002(03)01368-8.

[50] S. Abdullin et al., "The fast simulation of the CMS detector at LHC", *J. Phys. Conf. Ser.* **331** (2011) 032049, doi:10.1088/1742-6596/331/3/032049.

[51] C. Borschensky et al., "Squark and gluino production cross sections in pp collisions at $\sqrt{s}$ = 13, 14, 33 and 100 TeV", *Eur. Phys. J. C* **74** (2014) 3174, doi:10.1140/epjc/s10052-014-3174-y, arXiv:1407.5066.

[52] M. Czakon and A. Mitov, "Top++: A Program for the Calculation of the Top-Pair Cross-Section at Hadron Colliders", *Comput. Phys. Commun.* **185** (2014) 2930, doi:10.1016/j.cpc.2014.06.021, arXiv:1112.5675.

[53] P. Kant et al., "HATHOR for single top-quark production: Updated predictions and uncertainty estimates for single top-quark production in hadronic collisions", *Comput. Phys. Commun.* **191** (2015) 74, doi:10.1016/j.cpc.2015.02.001, arXiv:1406.4403.

[54] M. Aliev et al., "HATHOR: HAdronic Top and Heavy quarks crOss section calculatoR", *Comput. Phys. Commun.* **182** (2011) 1034, doi:10.1016/j.cpc.2010.12.040, arXiv:1007.1327.

[55] T. Gehrmann et al., "W^+W^- Production at Hadron Colliders in Next to Next to Leading Order QCD", *Phys. Rev. Lett.* **113** (2014) 212001, doi:10.1103/PhysRevLett.113.212001, arXiv:1408.5243.

[56] J. M. Campbell and R. K. Ellis, "An update on vector boson pair production at hadron colliders", *Phys. Rev. D* **60** (1999) 113006, doi:10.1103/PhysRevD.60.113006, arXiv:hep-ph/9905386.

[57] J. M. Campbell, R. K. Ellis, and C. Williams, "Vector boson pair production at the LHC", *JHEP* **07** (2011) 018, doi:10.1007/JHEP07(2011)018, arXiv:1105.0020.

[58] Y. Li and F. Petriello, "Combining QCD and electroweak corrections to dilepton production in FEWZ", *Phys. Rev. D* **86** (2012) 094034, doi:10.1103/PhysRevD.86.094034, arXiv:1208.5967.

[59] CMS Collaboration, "Top Tagging with New Approaches", CMS Physics Analysis Summary CMS-PAS-JME-15-002, 2016.

[60] ATLAS Collaboration, "Identification of high transverse momentum top quarks in pp collisions at $\sqrt{s}$ = 8 TeV with the ATLAS detector", *JHEP* **06** (2016) 093, doi:10.1007/JHEP06(2016)093, arXiv:1603.03127.

[61] M. Dasgupta, A. Fregoso, S. Marzani, and G. P. Salam, "Towards an understanding of jet substructure", *JHEP* **09** (2013) 029, doi:10.1007/JHEP09(2013)029, arXiv:1307.0007.

[62] A. J. Larkoski, S. Marzani, G. Soyez, and J. Thaler, "Soft Drop", *JHEP* **05** (2014) 146, doi:10.1007/JHEP05(2014)146, arXiv:1402.2657.

[63] Y. L. Dokshitzer, G. D. Leder, S. Moretti, and B. R. Webber, "Better Jet Clustering Algorithms", *JHEP* **08** (1997) 001, doi:10.1088/1126-6708/1997/08/001, arXiv:hep-ph/9707323.

[64] M. Wobisch and T. Wengler, "Hadronization corrections to jet cross sections in deep-inelastic scattering", (1998). arXiv:hep-ph/9907280.

[65] J. Thaler and K. Van Tilburg, "Identifying Boosted Objects with N-subjettiness", *JHEP* **03** (2011) 015, doi:10.1007/JHEP03(2011)015, arXiv:1011.2268.

[66] T. K. Ho, "Random decision forests", *Proceedings of 3rd International Conference on Document Analysis and Recognition* **1** (1995) 278, doi:10.1109/ICDAR.1995.598994.

[67] CMS Collaboration, "Performance of quark/gluon discrimination in 8 TeV pp data", CMS Physics Analysis Summary CMS-PAS-JME-13-002, 2013.

[68] CMS Collaboration, "Jet Performance in pp Collisions at 7 TeV", CMS Physics Analysis Summary CMS-PAS-JME-10-003, 2010.

[69] C. G. Lester and D. J. Summers, "Measuring masses of semi-invisibly decaying particles pair produced at hadron colliders", *Phys. Lett. B* **463** (1999) 99, doi:10.1016/S0370-2693(99)00945-4, arXiv:hep-ph/9906349.

[70] A. Barr, C. Lester, and P. Stephens, "A variable for measuring masses at hadron colliders when missing energy is expected; m(T2): the truth behind the glamour", *J. Phys. G* **29** (2003) 2343, doi:10.1088/0954-3899/29/10/304, arXiv:hep-ph/0304226.

[71] ATLAS and CMS Collaborations, "Procedure for the LHC Higgs boson search combination in summer 2011", Technical Report ATL-PHYS-PUB-2011-011, CMS NOTE-2011/005, 2011.

[72] A. L. Read, "Presentation of search results: the CL_s technique", *J. Phys. G* **28** (2002) 2693, doi:10.1088/0954-3899/28/10/313.

[73] T. Junk, "Confidence level computation for combining searches with small statistics", *Nucl. Instrum. Meth. A* **434** (1999) 435, doi:10.1016/S0168-9002(99)00498-2, arXiv:hep-ex/9902006.

[74] G. Cowan, K. Cranmer, E. Gross, and O. Vitells, "Asymptotic formulae for likelihood-based tests of new physics", *Eur. Phys. J. C* **71** (2011) 1554, doi:10.1140/epjc/s10052-011-1554-0, arXiv:1007.1727. [Erratum: doi:10.1140/epjc/s10052-013-2501-z].